ADVANCED FUNCTIONAL MATERIALS
www.afm-journal.de

www.MaterialsViews.com

Dependence of Dye Regeneration and Charge Collection on the Pore-Filling Fraction in Solid-State Dye-Sensitized Solar Cells

*Christian T. Weisspfennig, Derek J. Hollman, Christoper Menelaou, Sam D. Stranks, Hannah J. Joyce, Michael B. Johnston, Henry J. Snaith, and Laura M. Herz**

Solid-state dye-sensitized solar cells rely on effective infiltration of a solid-state hole-transporting material into the pores of a nanoporous TiO_2 network to allow for dye regeneration and hole extraction. Using microsecond transient absorption spectroscopy and femtosecond photoluminescence upconversion spectroscopy, the hole-transfer yield from the dye to the hole-transporting material 2,2′,7,7′-tetrakis(N,N-di-p-methoxyphenylamine)-9,9'-spirobifluorene (spiro-OMeTAD) is shown to rise rapidly with higher pore-filling fractions as the dye-coated pore surface is increasingly covered with hole-transporting material. Once a pore-filling fraction of ≈30% is reached, further increases do not significantly change the hole-transfer yield. Using simple models of infiltration of spiro-OMeTAD into the TiO_2 porous network, it is shown that this pore-filling fraction is less than the amount required to cover the dye surface with at least a single layer of hole-transporting material, suggesting that charge diffusion through the dye monolayer network precedes transfer to the hole-transporting material. Comparison of these results with device parameters shows that improvements of the power-conversion efficiency beyond ≈30% pore filling are not caused by a higher hole-transfer yield, but by a higher charge-collection efficiency, which is found to occur in steps. The observed sharp onsets in photocurrent and power-conversion efficiencies with increasing pore-filling fraction correlate well with percolation theory, predicting the points of cohesive pathway formation in successive spiro-OMeTAD layers adhered to the pore walls. From percolation theory it is predicted that, for standard mesoporous TiO_2 with 20 nm pore size, the photocurrent should show no further improvement beyond an ≈83% pore-filling fraction.

1. Introduction

Dye-sensitized solar cells (DSSCs) offer a promising route towards production of cost-effective photovoltaic systems with low construction energy requirements.[1,2] Here, a dye sensitizer absorbs incident sun light, followed by electron injection into a mesoporous metal-oxide electrode and dye regeneration. For the latter step, DSSCs have conventionally incorporated an iodide/triiodide (I^-/I_3^-) liquid electrolyte as a redox mediator.[3] However, the possibility of solvent leakage and corrosion and the low redox potential of I^-/I_3^- have limited further efficiency improvements of DSSCs.[4,5] To overcome these issues, cobalt complex redox mediators have recently been demonstrated which achieve power-conversion efficiencies of up to 12%.[6] In an alternative approach, a solid-state hole-transporting material (HTM) is employed to replace the liquid electrolyte, which also opens the possibility for flexible, all-solid solar cells. Here, the most commonly and successfully used HTM has been 2,2′,7,7′-tetrakis(N,N-di-p-methoxyphenylamine)-9,9'-spirobifluorene (spiro-OMeTAD).[7] However, despite significant improvements over the last two decades, the performance of solid-state DSSCs using spiro-OMeTAD has not surpassed a power-conversion efficiency of 7.2% which is lower than that of the best cells employing liquid-electrolytes.[8] The main reason for this discrepancy is that solid-state DSSCs show optimized performance at relatively low layer thickness of only ≈2 μm, which limits light harvesting efficiencies.[9] It has been proposed that crucial limitations to layer thicknesses are the intrinsically low mobility of spiro-OMeTAD[10] and incomplete filling of the mesoporous TiO_2 pores with the hole-transporting material.[11–13] Conceptually, a high pore-filling fraction (PFF) should be required to allow both efficient dye regeneration by hole transfer to the HTM, and to offer percolation pathways for holes to the cathode for effective charge collection.

Filling of the pores is commonly achieved by deposition of a solution of spiro-OMeTAD on top of the mesoporous TiO_2 network layer followed by spin coating. During this process, the solution can initially penetrate into the pores and achieve a PFF proportional to the initial volume concentration of the solution. However, once the solvent begins to evaporate, the remaining solution on top of the TiO_2 can act as a reservoir and increase

C. T. Weisspfennig, D. J. Hollman, C. Menelaou, Dr. S. D. Stranks, Dr. H. J. Joyce, Dr. M. B. Johnston, Dr. H. J. Snaith, Prof. L. M. Herz
Clarendon Laboratory
Department of Physics
University of Oxford
Parks Road, Oxford, OX1 3PU, UK
E-mail: l.herz1@physics.ox.ac.uk

The copyright line of this paper was amended 19 January 2016.

This is an open access article under the terms of the Creative Commons Attribution License, which permits use, distribution and reproduction in any medium, provided the original work is properly cited.

DOI: 10.1002/adfm.201301328

© 2013 The Authors. Published by WILEY-VCH Verlag GmbH & Co. KGaA, Weinheim

the spiro-OMeTAD concentration in the pores by filling the space previously occupied by the evaporated solvent. Thus, PFFs higher than the initial volume concentration of the solution can be achieved,[14] although in reality a value of 100% is unattainable because some vacant space will be left in the pores as the solvent evaporates.[14,15]

Despite the clear importance of pore filling on the device efficiency, its precise influence on the hole-injection and charge-collection efficiency is not well understood. Initial studies suggested that for optimized devices, hole transfer from the dye to the HTM occurs with efficiencies of near unity, even though pore filling is not fully complete.[11,16] These findings agree with a suggestion that complete hole transfer should be possible once the entire TiO_2 surface is covered with at least a single layer of spiro-OMeTAD[15] which does not require full filling of the pore. However, lower PFFs might still achieve close to complete hole-transfer yields, if holes can diffuse through the dye network before transferring to the HTM.[17] In addition, a sufficiently high PFF is required to ensure optimized charge collection towards the electrodes. Device studies suggest that for these reasons, a PFF of at least 60% is necessary to achieve optimized device performance.[18] However, the overall picture of how the hole-transporting material arranges inside the pores upon solvent evaporation, and the subsequent effect on charge migration, are still a matter of debate.

We present here a complementary spectroscopic and device investigation into the effect of pore-filling fraction on solid-state DSSCs incorporating a TiO_2 mesoporous electrode sensitized with a Ruthenium dye, and spiro-OMeTAD as the HTM. We first apply a combination of microsecond transient absorption and femtosecond photoluminescence (PL) spectroscopies from which we are able to gain crucial insights into both the yield of hole transfer from the dye to the HTM, and the mode of arrangement of the HTM in the pore. We find that the hole-transfer yield improves rapidly with increasing PFF and reaches a maximum at a value of only ≈30%, in agreement with hole diffusion within the dye network preceding hole transfer to the HTM. Moreover, we obtain information on the HTM layer arrangement within the pore by applying simple Monte Carlo techniques to replicate the observed transfer of charges at the dye:HTM interface, and the movement of excitations through the HTM material. These combined spectroscopic studies reveal that HTM filling of the pore can be modeled through successive layer build-up of molecules assuming random positions on the pore wall. We subsequently correlate these findings with performance data for a matching set of full DSSCs. We observe a series of sharp onsets in both device photocurrent and efficiency with increasing pore-filling fraction. By applying percolation theory, we show that these onset points have excellent correspondence with the formation of complete charge collection pathways in successive layers of such randomly positioned hole-transporting molecules on the pore wall. While the formation of a full charge percolation pathway in the first HTM monolayer is clearly essential for extraction of any photocurrent, pathway completion in subsequent layers may give further step-change in photocurrent because these offer shorter routes located further away from an interface at which charge recombination losses can occur. By modeling such pathway completion we are hence able to predict from percolation theory how pore-filling fractions must be tailored for optimized device performance.

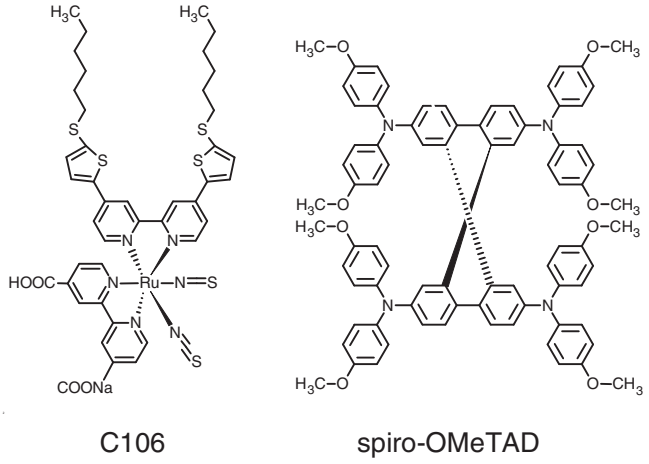

Figure 1. Chemical structures of the dye sensitizer NaRu(4,4′-bis(5-(hexylthio)thiophen-2-yl)-2,2′-bipyridine)(4-carboxylic acid-4′-carboxylate-2,2′-bipyridine)(NCS)2, known as C106, and the hole-transporting material 2,2′,7,7′-tetrakis(*N*,*N*-di-p-methoxyphenylamine)-9,9′-spirobifluorene (spiro-OMeTAD) employed in the DSSCs investigated in this study.

2. Results and Discussion

Figure 1 shows the chemical structures of the molecular materials incorporated in the investigated DSSC devices. NaRu(4,4′-bis(5-(hexylthio)thiophen-2-yl)-2,2′-bipyridine)(4-carboxylic acid-4′-carboxylate-2,2′-bipyridine)(NCS)2, known as C106,[19] is used as a dye sensitizer forming a monolayer on a TiO_2 network with pores of average diameter $d_{pore} \approx 20$ nm[20] that are partially infiltrated with spiro-OMeTAD as the hole-transporting material. Two sets of samples with varying PFF were prepared in parallel, one for spectroscopic measurements and another for device measurements, as described in detail in the Experimental Section. The sample sets only differed in that for those used in spectroscopy, quartz substrates were used (instead of FTO) and the deposition of silver electrodes was omitted. Samples were prepared for 14 different volume concentrations of spiro-OMeTAD in solution ranging from 0% to 20% to cover the maximum accessible range of PFFs. The actual PFF resulting from these solution concentrations can be quantified by one of several techniques.[14,15,18] In the method chosen here, the PFF is calculated from the sum of the spiro-OMeTAD volume concentration present in the pores before solvent evaporation, and the increase in concentration due to further infiltration during evaporation.[14] The former is equal to the volume concentration c of spiro-OMeTAD in the initial solution while the latter is inferred from the difference in the amount of spiro-OMeTAD on top of the TiO_2 before and after evaporation, divided by the volume of the pores. Here, the amount of spiro-OMeTAD before evaporation can be calculated from the product of the thickness d_{sol} of the deposited solution layer on top of the TiO_2 and the solution concentration c. The amount of HTM present after evaporation is given by the thickness of the resulting solid

© 2013 The Authors. Published by WILEY-VCH Verlag GmbH & Co. KGaA, Weinheim

capping layer d_{cl}. The volume of the pores is determined by the product of porosity p and thickness d of the TiO_2 mesoporous network layer. The PFF can thus be calculated using[14]

$$PFF = c + \frac{d_{sol}c - d_{cl}}{dp} \quad (1)$$

For these calculations, the thickness d_{sol} and the porosity p were taken to be 6.9 ± 0.5 µm and 49 ± 1%, respectively.[18] The thickness d of the TiO_2 network and the capping layer d_{cl} were measured for each sample through cross-sectional SEM imaging, as shown in Supporting Information. Using this method, pore-filling fractions ranging from 0–67% were accessible in our study.

As a first assessment, we investigate spectroscopically how the pore-filling fraction affects the efficiency of hole transfer from the dye sensitizer to the hole-transporting material. Primary electron transfer from the photoexcited dye into the TiO_2 occurs on the femto- to pico-second time scale.[21,22] The subsequent hole transfer from the dye onto the HTM has been shown to cover a broad time range from pico- to nano-seconds.[16] As required, hole injection is hence several orders of magnitude faster than the competing recombination process between the dye cation and an electron present in TiO_2, which occurs on the micro- to millisecond timescale.[23–25] Microsecond transient absorption spectroscopy therefore provides an excellent tool to quantify hole-injection efficiencies as well as the subsequent recombination dynamics[26,27] by probing for the presence or absence of absorption features associated with the neutral or charged states of the dye or HTM.

For measurements presented here, samples were photoexcited at a wavelength of 550 nm as this coincides with an absorption peak of C106 as well as an absence of absorption from spiro-OMeTAD. At the employed probe wavelength of 520 nm two main contributions to the signal arise, which are photoinduced absorption (PA) from the spiro-OMeTAD radical cation[16,28] and photobleaching (PB) of the ground-state absorption of the dye[29] caused by the presence of neutral or charged species on the dye. **Figure 2** displays microsecond absorption spectroscopy transients for samples with a range of different pore-filling fractions. At early times within the observation window (1–2 µs) the signal is relatively constant and it hence reflects the period after which any charge exchange at the TiO_2:dye:HTM interface will have occurred, but before any subsequent recombination has become evident. For the sample containing no HTM (i.e., 0% PFF) the negative signal arises solely from PB of the dye cations, while for samples with non-zero PFF, the signal is a combination of negative PB from dye cations for which hole transfer has not been feasible, and positive PA from HTM molecules that have received a hole. Hence we are able to determine the hole-transfer yield as a function of the pore-filling fraction by referencing the initial (1–2 us) change in optical density ΔOD for a sample of given PFF against ΔOD_{dye} for the sample containing no HTM:[16,27,30]

$$\text{Yield} = \left(1 - \frac{\Delta OD}{\Delta OD_{dye}}\right)\left(1 + \frac{\varepsilon_{HTM^+}}{\varepsilon_{dye^+} - \varepsilon_{dye^0}}\right)^{-1} \quad (2)$$

Here, ε_{HTM+} is the extinction coefficient of cations in the HTM, and ε_{dye+}–ε_{dye0} is the difference between the extinction

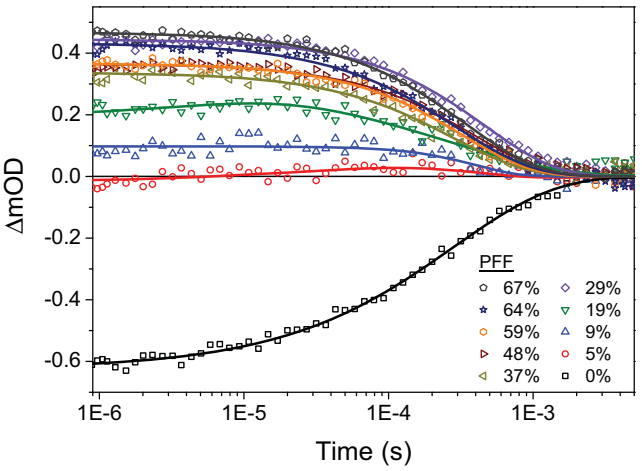

Figure 2. Microsecond transient absorption dynamics of TiO_2/C106/spiro-OMeTAD samples with varying pore-filling fractions measured at a probe wavelength of 520 nm. The samples were excited at 550 nm with a fluence of 50 uJ cm^{-2}. Results are averaged over those obtained from two samples with identical pore-filling fraction. For the transients displayed, no ionic tBP or Li-TFSI salts had been added to the materials (curves for samples containing additives are shown in Supporting Information). The solid lines are guides to the eye.

coefficients of cations and the ground-state of the dye. Qualitative inspection of the early-time transient absorption signal (Figure 2) shows that the hole-injection yield into the HTM initially rises rapidly but then saturates with increasing PFF. The subsequent decay dynamics of the transient absorption signal are dominated by charge recombination across the interface. For the sample containing no HTM, the observed reduction of dye cation PB is attributed to recombination with electrons in the TiO_2. The half-reaction time is extracted as ≈160 us, which is similar to lifetimes reported for use of the alternative dyes cis-Bis(isothiocyanato)(2,2′-bipyridyl-4,4′-dicarboxylato)(4,4′-di-nonyl-2′-bipyridyl)ruthenium(II) (Z907) and Ru^{II}(2,2′-bipyridyl-4,4′-dicarboxylate)$_2$(NCS)$_2$ (N3).[31,32] For samples with high PFF the observed dynamics similarly reflect charge recombination across the TiO_2:dye:HTM interface. Here, half-reaction times appear to be quite similar to those observed in the absence of HTM, which is because in the absence of ionic additives, cations in spiro-OMeTAD tend to remain localized close to the charge-generating surface.[33] It should be noted that in order to determine the fundamental properties of the hole-injection process all of the measured samples were prepared without ionic additives. However, both liquid-electrolyte and solid-state dye-sensitized solar cells are known to show a substantial enhancement of the power-conversion efficiency after addition of ionic additives such as lithium bis(trifluoromethylsulfonyl)imide salt (Li-TSFI) and 4-tert-Butylpyridine (tBP).[26,34–37] Thus, to determine the influence of additives on the hole-transfer yield, we performed the same transient absorption experiment with samples containing varying concentrations of tBP and Li-TFSI and varying PFFs. While a change in decay dynamics is visible, we observed no significant dependence of the hole-transfer yield on the concentration of tBP and Li-TFSI (see Supporting Information) within the experimental error. We hence conclude that while charge recombination dynamics are, as expected, affected

© 2013 The Authors. Published by WILEY-VCH Verlag GmbH & Co. KGaA, Weinheim

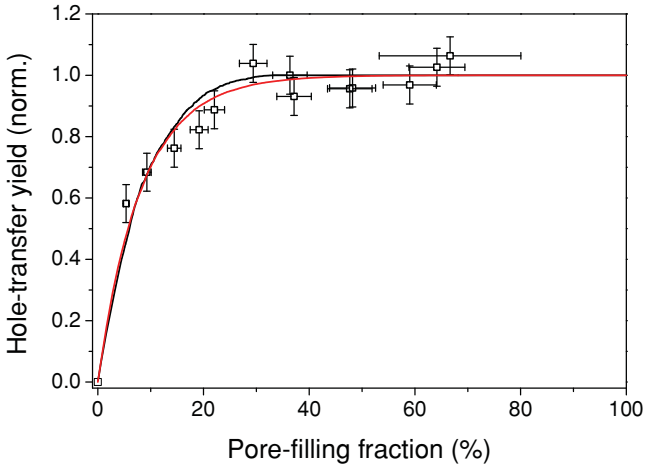

Figure 3. Normalized yield of hole transfer from dye cation to spiro-OMeTAD obtained by applying Equation 3 to the data displayed in Figure 2 averaged over the time interval of 1–2 µs. The solid lines are a fit to the data using a simple infiltration model assuming conformal coating (black) and random placement (red) of spiro-OMeTAD molecules onto the pore walls and the possibility for lateral "dye-hopping" of the hole prior to transfer to spiro-OMeTAD.

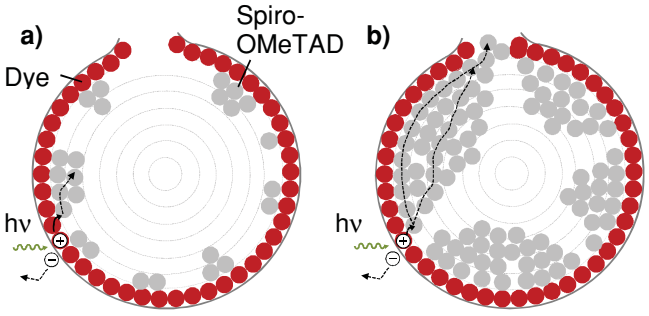

Figure 4. Cross-sectional sketch of an idealized pore within the TiO_2 network containing a monolayer of dye (red circles) and randomly distributed spiro-OMeTAD molecules (grey circles) attached to the surface. The grey dashed lines indicate the different layers of spiro-OMeTAD while the black dashed lines mark possible diffusion pathways of the photogenerated hole. a) Low pore-filling fraction: A complete pathway does not exist and the hole is thus not able to escape out of the pore. b) High pore-filling fraction: a sufficient number of spiro-OMeTAD molecules have infiltrated into the pore to form a percolation path allowing the hole to escape. The diffusion path length depends on the number of layers that have reached percolation threshold. Due to the shape of the pore, higher layers will provide a shorter pathway and subsequently increase the probability of the hole to escape before recombination occurs.

by ionic additives, hole-transfer yields appear to be largely independent and we will therefore ignore these effects for the remainder of the discussion.

Figure 3 shows the yields of hole transfer from dye to HTM as a function of pore-filling fraction, as extracted from the early-time transient absorption signals using Equation 2. For very low PFFs, a rapid increase of the hole-transfer yield is visible, however, beyond a PFF of 30% no further significant changes are observed. This trend can be understood by considering the infiltration process of spiro-OMeTAD into an idealized pore of the TiO_2 network coated by a monolayer of dye, as schematically shown in **Figure 4**. It is reasonable to assume that for the yield of hole transfer from the dye to the infiltrated HTM, only the surface coverage provided by the first monolayer of HTM will matter. We calculate the fraction of HTM molecules contained in this first layer for a completely filled pore (100% PFF) to be 33%, using a spiro-OMeTAD density[14,18] of 1.02 g cm^{-3} and an average TiO_2 pore diameter d_{pore} of 20 nm.[20] In this simple model, the HTM takes up a cubic cell of volume 2 nm^3 with a side length of 1.26 nm. The projected area of the dye is assumed to be 1.7 nm^2, identical to that of the very similar dye Z907.[38] Two main factors will determine how the hole-transfer yield depends on PFF, which are the HTM layer morphology created as the pores are filled, and the extent to which lateral hole-hopping from one dye molecule to another occurs prior to hole transfer to the HTM. The very simplest model in terms of analytical effort would assume conformal coating (i.e. each HTM layer is completed before the next one is allowed to form) and absent lateral dye-to-dye hole-hopping. In accordance with our calculation above, this case would require a PFF of 33% to achieve complete hole transfer, which happens to be in close agreement with the experimentally observed yield saturation at ≈30% PFF. However, given that significant diffusion within such dye sensitizer monolayer has in fact been observed,[17] and considering the amorphous nature of spiro-OMeTAD[39,40] we believe that this model is somewhat too simplistic and diffusion within the dye before hole transfer occurs will need to be taken into account.

The exact film formation of spiro-OMeTAD within a TiO_2 pore is unknown, hence we aim to approximate reality by the use of three simplified model scenarios which can be compared against each other for their effectiveness in reproducing the experimental data sets. These cases rely on the relative effects of surface tension and surface energy minimization at the wall of a nanopore. In the first case, HTM molecules are free to move around after initial attachment to the pore wall until an overall potential minimum has been found; in addition, a HTM molecule prefers to stick to itself more than to the pore wall. As a result, spheres or pseudo spheres form. In the second case, HTM molecules are again free to move around after initial attachment to the pore wall, however the HTM prefers to stick to the pore wall more than to itself; conformal coating results. For the third case, HTM molecules do not move around significantly after initial attachment to the pore wall, that is, HTMs enter the pore and stick somewhere random. We can rule out the first case on the basis of a previous study, showing that surface tension of solution-dropped spiro-OMeTAD on a TiO_2 surface is low.[12] We have modeled the experimentally observed hole-transfer yields for the remaining two cases as follows. For the case of conformal coating, molecules will coat the inner surface of the pore first. Once the entire surface is covered with spiro-OMeTAD, the subsequent molecules settle in the second layer on top of the first one. This process is repeated until the pore is filled completely, and simulated through a Monte Carlo approach described in Supporting Information. Random infiltration, on the other hand, leads to simultaneous filling of several layers, which is modeled by molecules assuming a random position available at the surface (see Supporting Information).

© 2013 The Authors. Published by WILEY-VCH Verlag GmbH & Co. KGaA, Weinheim

This position may hence be directly at the dye monolayer, or, in case that this specific surface position is already covered by a spiro-OMeTAD molecule, on top of the existing molecule to contribute to a second, third or subsequent layer. From these Monte Carlo simulations we are able to estimate the resulting percentage p(PFF) of the dye surface covered with spiro-OMeTAD molecules for different PFFs and both models (see Supporting Information). In case of absent lateral hole-hopping, the hole-transfer yield would be equal to the simulated surface coverage. However, lateral dye hole-hopping is likely to be particularly significant for devices with very low PFFs and can be taken into account by considering the average number $n(t)$ of distinct dye molecules a hole is able to visit within a given time t between its creation and transfer to the HTM. In the case of the random placement model, from a simple statistical consideration of the hole hopping process (see Supporting Information) we hence find that the expected hole-transfer yield η_{ht} depends on p(PFF) and $n(t)$ through

$$\eta_{ht}(\mathrm{PFF}) = 1 - \left[1 - p(\mathrm{PFF})\right]^{n(t)+1} \quad (3)$$

where it is assumed that $n(t)$ is much smaller than the number of possible spiro-OMeTAD molecules in the surface layer. Since the fractional dye coverage in HTM (p(PFF)) is already determined from the Monte Carlo simulation, the number $n(t)$ of dye molecules visited by the hole can be extracted by fitting Equation 3 to the experimental data shown in Figure 3. For the conformal coating model the hole-transfer yields have to be extracted from a Monte Carlo simulation. Taking these assumptions, we find that the best fits are achieved for both models using a value of $n = 3$. This results in a mean-square displacement of approximately 5.5×10^{-14} cm^2 for a random hole walk. Using the equation $\langle r^2 \rangle = 4Dt$, we derive a diffusion coefficient D of 6.8×10^{-9} cm^2 s^{-1}. This value is in very reasonable agreement with a comparison value[17] of 4.1×10^{-9} cm^2 s^{-1} from previous studies of hole diffusion through a layer of Z907, a dye very similar to C106. Comparing the resulting simulated dependencies of the hole-transfer yield on PFF (Figure 3) we find that only small differences are visible between the two infiltration models. Hence the simulation indicates that the resulting hole-transfer yield and the extracted extent of dye-dye hopping appear to be robust with respect to the exact choice of infiltration process. Our results and simulations suggest that because of dye-dye hole-hopping, hole transfer to the HTM can be completed even for low PFFs within only a few us, which is several times faster than the competing half-reaction time of the recombination process (≈160 us). For even lower PFF, complete hole transfer might still be possible, if the required time for hole hopping on the dye is sufficiently shorter than ≈160 µs. We note here that inter-dye hole-hopping is likely to play a critical role in polymer HTM based DSSCs, where good operation with PFFs as low as 7% have been observed.[41]

While simulations of the hole-transfer yield were relatively unrevealing of spiro-OMeTAD morphology in the pore, we are able to perform an alternative set of spectroscopic measurements which is directly sensitive not only to the arrangement of the first HTM monolayer on the dye, but also probes the presence of higher layers. In these femtosecond photoluminescence upconversion (PLUC) experiments, excitons are

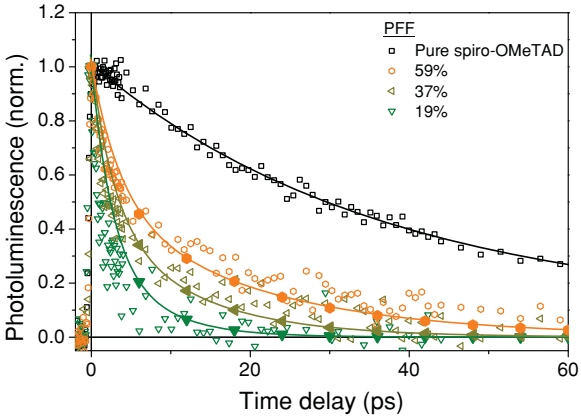

Figure 5. Femtosecond photoluminescence upconversion dynamics (hollow symbols) of TiO_2/C106/spiro-OMeTAD samples with varying pore-filling fractions at a detection wavelength of 430 nm (spiro-OMeTAD emission). The samples were excited at 400 nm with a fluence of 30 nJ cm^{-2}. The solid symbols show the results of a Monte Carlo simulation using random placement of spiro-OMeTAD molecules as described in the text, with the connecting solid lines as a guide to the eye.

uniformly photo-excited in the spiro-OMeTAD molecules and diffuse through the network until they either recombine or come in proximity to the dye surface where they undergo energy or charge transfer. The lifetime of the photogenerated excitons will therefore depend on the structure of the spiro-OMeTAD network and can be compared to determine whether a conformal coating or a random infiltration model is more appropriate. For low PFFs, excitons will be generated close to the surface and thus be quenched quickly. In contrast, for high PFFs the average distance from exciton position to dye network will be larger, resulting in a longer lifetime.

Figure 5 shows the photoluminescence emitted from pore-infiltrated spiro-OMeTAD following its preferential excitation at 400 nm. A clear dependence of the exciton recombination lifetime in spiro-OMeTAD on the PFF can be seen. Also shown are the results of a Monte Carlo simulation based on the previously introduced model of random infiltration providing the structure of the spiro-OMeTAD network. Exciton dynamics are simulated using typical assumptions:[42–44] In the first step, excitons are placed on random spiro-OMeTAD molecules within the network. Migration is then modeled using a random walk to one of the neighboring molecules. If an interface between dye and spiro-OMeTAD is reached, perfect quenching is assumed. In contrast, if the exciton reaches a non-quenching interface, perfect reflection occurs. To account for the natural recombination life time of excitons, the simulated results were multiplied with the fitted decay response of a sample containing only spiro-OMeTAD. Using these assumptions and a hopping rate of 6 ps between two spiro-OMeTAD molecules, the simulated PL decay curves for the random placement model show excellent correspondence with the experimentally measured exciton population dynamics. In the case of a conformal coating model, however, all samples with a PFF below 33%, that is, the PFF at which the surface layer is fully covered and higher layers would just begin to fill up, are expected to show the same dynamics. This lies in contrast to the experimentally found dynamics and

© 2013 The Authors. Published by WILEY-VCH Verlag GmbH & Co. KGaA, Weinheim

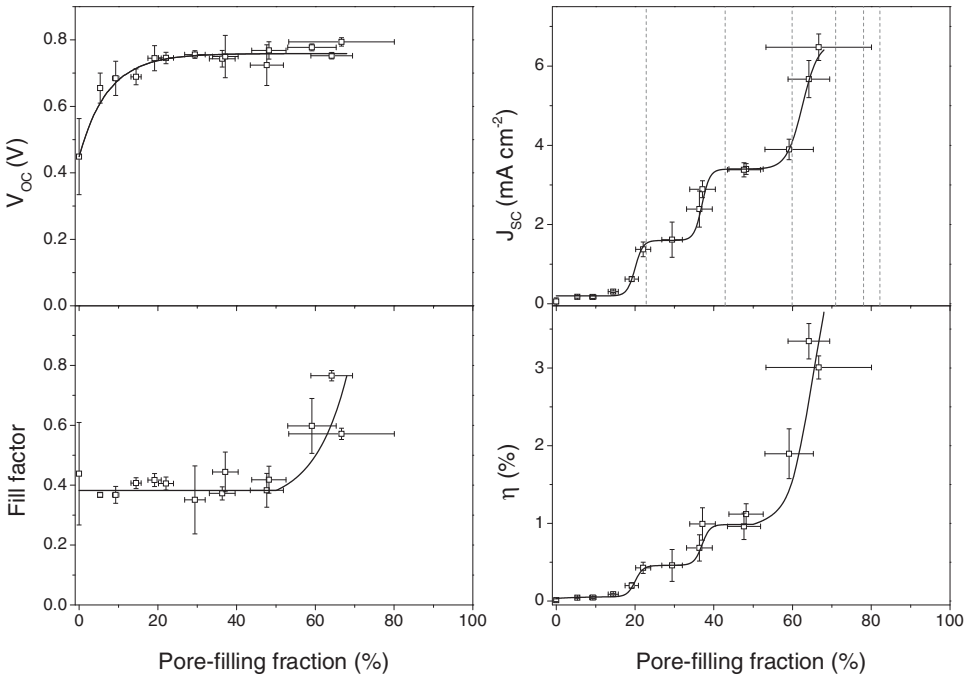

Figure 6. Characterization data for complete solid-state DSSC devices as a function of pore-filling fractions. Top left: Open-circuit voltage (V_{oc}). Top right: Short-circuit current (J_{sc}). Bottom left: Fill factor. Bottom right: Power-conversion efficiency (η). The solid lines are guides to the eye. The dashed lines in the figure showing the short-circuit current indicate the expected positions of the onsets as predicted by percolation theory using a model of random infiltration of spiro-OMeTAD molecules. Results are averaged over 5–6 devices and error bars for V_{oc}, J_{sc}, fill factor, and η reflect the standard deviation. These devices contain additives tBP and Li-TFSI, whose concentration was held constant in the solution, rather than with respect to the spiro-OMeTAD concentration, in order to ensure constant charge injection across all devices.[49–52]

suggests that a substantial amount of spiro-OMeTAD molecules is present in higher layers before the surface layer is fully covered. These experiments suggest that the model of random successive site selection of spiro-OMeTAD molecules entering the pore is the more suitable model of the two extreme examined cases. This tends to suggest that while in reality some molecular re-arrangement may well occur, minimization of the overall energy associated with the HTM arrangement appears to be incomplete in these nanopores. We hence conclude that while the reality may lie between the two extreme cases of random HTM placement and conformal coating, the former describes the available data much better.

With such knowledge gained from spectroscopic insights on the HTM distribution it is now highly interesting to determine the effects on photovoltaic device performance. **Figure 6** shows the dependence on PPF of the open-circuit voltage (V_{oc}), short-circuit current (J_{sc}), fill factor (FF), and power-conversion efficiency (η) for DSSCs matching the sets used for the spectroscopic investigations. As discussed earlier, the two main mechanisms influenced by the fraction of pore filling with HTM are the yield of hole transfer from the dye and the subsequent hole extraction through the HTM to the electrode. We find that the open-circuit voltage V_{oc} shows the same dependence on the PFF as the hole-transfer yield (Figure 3) suggesting a clear correlation between charge build-up in the HTM and increasing open-circuit voltage, or splitting of the Quasi Fermi levels, in the device. The fill factor, short-circuit current and power-conversion efficiency on the other hand, show different trends, including sharp increases at higher pore-filling fractions. The fill factor is constant up to a PFF of ≈60% and shows a sharp rise beyond this value. Interestingly, the short-circuit current and power-conversion efficiency display steps of superlinear increases with distinct onsets at PFFs of ≈20%, ≈37%, and ≈63%. These may be explained by considering that short-circuit current generation relies on efficient hole extraction, which requires a complete pathway through the spiro-OMeTAD network to the counter electrode. At low PFFs, isolated spiro-OMeTAD molecules as well as isolated clusters will exist preventing holes on these molecules from being extracted. Once higher PFFs are achieved spiro-OMeTAD molecules will be in close enough proximity to enable diffusion of the holes to the counter electrode as illustrated schematically in Figure 4.

The step-like increases of photocurrent with PFF can be understood from percolation theory[45] considering a network where each position is randomly filled with a molecule according to a certain probability. Here, a "critical probability" p_c or ratio of unfilled to filled positions exists, beyond which diffusion through the entire network is possible from almost any molecule within the network and below which such percolation becomes almost impossible. Thus, at PFFs below p_c negligible short-circuit current is expected, whereas beyond p_c the value of the short-circuit current should display a sharp photocurrent onset as observed. The occurrence of several such onsets, as seen in Figure 6, can be explained by considering the specific random infiltration process that leads to successive layer build-up. For holes to have the possibility to diffuse out of

© 2013 The Authors. Published by WILEY-VCH Verlag GmbH & Co. KGaA, Weinheim

the pore, only the surface layer needs to reach the critical ratio p_c since it will then offer a complete path from each starting position to the counter electrode. Due to the random infiltration process, p_c is first reached in this surface layer and hence the first onset with PFF will originate from this layer. Once the second layer reaches p_c, an additional sharp onset in photocurrent ought to be expected because this layer offers a better pathway to holes than the first, for two reasons. First, the holes migrating through higher layers will spend more time further away from the TiO_2:dye surface which reduces their probability of recombination with electrons in the TiO_2, and second, due to the curved shape of the pore the path length to the counter electrode will be reduced for such higher layers, as indicated in Figure 4. For analogous reasons, onsets are expected to occur every time the critical ratio p_c is reached in a forming, higher-lying layer.

Our experimental observations of photocurrent onsets show that up to the achieved PFF of 67% three successive layers of spiro-OMeTAD reach percolation threshold. We can compare the observed photocurrent onsets with theoretical expectations from percolation theory assuming that completely occupied spiro-OMeTAD layers can be approximated by a 2-dimensional lattice in which each molecule is surrounded by six adjacent molecules to which a hole can be transferred to. For this case the critical ratio p_c can analytically be found[46] to be 0.5, that is, 50% of the positions in a layer would need to be filled with spiro-OMeTAD to create sufficient percolation pathways for holes. We can determine the PFFs for which these thresholds are reached from the results of our Monte Carlo simulation of layer build-up through placement of molecules at random positions, as discussed earlier and shown in Supporting Information. We find that for the given pore size of 20 nm, percolation pathway completions should theoretically occur at 23%, 43% and 60% for the first (surface), second and third layer away from the dye interface, respectively. These values are in good agreement with the experimentally found onsets of the photocurrent at ≈20%, ≈37%, and ≈63% PFF. Deviations from the experimental data may be caused by non-idealized shapes and diameters of the pores, systematic errors of the PFF measurement, and deviations of the actual spiro-OMeTAD arrangement from the idealized assumptions of entirely random infiltration. Formation of pathways between previously isolated pores or clusters of pores within the TiO_2 network might also influence charge collection.

Given the good agreement of photocurrent onsets with predictions from percolation theory, we may now explore theoretical predictions that may be gained from this simple model. For example, while higher PFFs than ≈67% could not be accessed experimentally here, additional onsets are expected at 71%, 78%, 82%, and 83% PFF. Thus, beyond 83% PFF, no further significant increases of the short-circuit current would be expected, as this represents the threshold at which the last layer fitting into the pore reaches percolation threshold. Interestingly, changing the pore size in the TiO_2 network would be expected to change the position of these photocurrent onsets. We are able to simulate this effect by again using the simple Monte Carlo simulation of random successive positioning of HTM on the pore surface. **Figure 7** shows the calculated PFF required to reach a 50% occupancy of available positions in a given layer as a function of pore diameter. Within this description, each line is expected to contribute to a rise in associated photocurrent for a given pore size and hence the highest available layer envelope will define the PFF beyond which no further photocurrent increases are to be expected. Figure 7 demonstrates that for pores with a 30 nm diameter the last onset in photocurrent is expected at 92% PFF, while for a 10 nm size pore the last onset would occur at 64% PFF. Conceptually, the increase in the highest percolation threshold onset with increasing pore size can be understood considering that for a small pore fitting just one monolayer of HTM, a 50% PFF would be sufficient to reach the envelope line. For a pore fitting two layers on the other hand, the second layer would have 50% coverage which, by the successive infiltration process, would yield a first layer with coverage higher than 50% and hence the total PFF required for the second onset would be higher than 50%. For these reasons, the PFF at which the highest percolation threshold occurs will generally increase with pore size. Due to the possibility of non-random infiltration at higher layers or non-idealized pore shapes, however, the absolute value of the overall PFF required to reach percolation threshold in all layers might in reality deviate slightly from the model. Our simple model hence predicts that tuning the pore size may be an important tool to achieve optimized short-circuit current in cases where the PFF is limited, such as for devices with higher TiO_2 layer thicknesses.

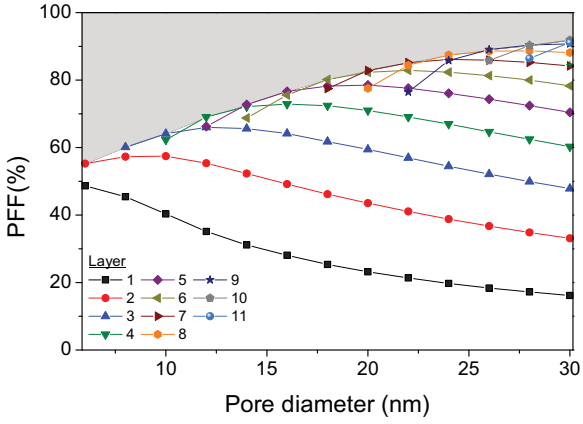

Figure 7. Simulated pore-filling fractions at which an onset of the short-circuit current is expected. At these points 50% of a layer is occupied with spiro-OMeTAD molecules which as predicted by percolation theory is the lowest value at which a diffusion pathway through the layer exists. In case of the first layer, this diffusion pathway gives holes a new route from the dye-HTM interface to the electrode. In case of subsequent layers, a shorter route to the electrode located further away from an interface at which charge recombination losses can occur becomes available which should result in a further increase of the short-circuit current. The solid lines are a guide to the eye. The shaded area indicates the PFF range for which no further improvement of the short-circuit current is expected because the percolation threshold for the highest available layer in the pore has already been reached.

3. Conclusions

In conclusion, we examined the dependence of dye regeneration and charge collection on the pore-filling fraction (PFF) in

© 2013 The Authors. Published by WILEY-VCH Verlag GmbH & Co. KGaA, Weinheim

dye-sensitized solar cells by a combined approach employing spectroscopic and device performance measurements. Using microsecond transient absorption spectroscopy, we find that the yield of hole transfer from the dye sensitizer to spiro-OMeTAD hole transporter increases rapidly with increasing pore-filling fractions but saturates at ≈30% PFF. We propose simple models to describe filling of the dye-sensitized TiO_2 pores focus on the two extreme cases. We simulate (i) successive build-up of spiro-OMeTAD molecules that attach to a random positions on the pore wall or an already attached spiro-OMeTAD molecule, if present and (ii) conformal coating in which the lowest layer is always filled first. We show that for both coating types for the of pore walls in spiro-OMeTAD, the experimentally determined hole-transfer yield suggest that holes located on dye molecules must undergo lateral hole-hopping, visiting on average 3 dye molecules before transferring to spiro-OMeTAD. As a result, only a relatively small pore-filling fraction is required to achieve efficient hole transfer from dye sensitizer to spiro-OMeTAD hole transporter. We further experimentally examine the validity of both pore-infiltration models by by using femtosecond photoluminescence transient spectroscopy in which spiro-OMeTAD is directly excited and the quenching of its re-emission caused by charge or energy transfer to the dye is observed. This technique is highly sensitive to the layer build-up of HTM inside the pore as it determines the time scales on which excitations generated in a random spiro-OMeTAD molecule can diffuse to the dye:spiro-OMeTAD interface. Applying a simple Monte Carlo approach to simulating such excitation transfer based on the random infiltration model gives excellent agreement with data. The conformal coating model, on the other hand, is incompatible with the observed slowing of the PL transients at a low PFF threshold, for which it does not predict the presence of secondary layers. These experiment suggest that the HTM molecular build-up on the pore walls is relatively random and HTM molecules may not have the facility to move until the overall positioning energy is minimized. We correlate the findings obtained from spectroscopic measurements with performance data for complete solar cell devices. We find that the open-circuit voltage saturates around ≈30% PFF, closely following the dependence of hole-transfer yield on the PFF and suggesting a correlation between charge build-up in the HTM and increasing open-circuit voltage In contrast, the short-circuit current and power-conversion efficiency show steps of super-linear increases with distinct onsets at PFFs of ≈20%, ≈37%, and ≈63%. We demonstrate that these thresholds correspond to PFF values at which formation of percolation pathways would theoretically be expected to occur for the lowest three layers of spiro-OMeTAD coating the pore walls in the way described by the random infiltration model. Percolation theory for a two-dimensional lattice of molecules in triangular arrangement predicts relatively sudden formation of continuous pathways at 50% occupancy hence explaining the onset of photocurrent at the observed PFFs. The observation of multiple onsets in the photocurrent also demonstrates that layers further away from the dye: TiO_2 must offer better charge routes out of the pore, possibly because they are shorter by geometry, but also because they offer routes further away from an interface at which charge recombination may occur. Our simple model of random pore filling predicts that the PFF required for a complete percolation pathway in the outermost layer of spiro-OMeTAD, and hence the PFF beyond which no further enhancement in photocurrent is to be expected, should increase with increasing pore diameter. These findings offer a new level of understanding of the pore infiltration mechanism in solid-state dye sensitized solar cells and its effect on the overall performance of these devices through both sensitizer regeneration and charge transport towards the electrodes.

4. Experimental Section

Sample Preparation: The following procedure was performed for fabrication of samples for device measurements. Fluorine doped tin oxide (FTO) glass (15 Ω/sq, Pilkington) was etched for the appropriate electrode pattern with Zn powder and HCl (2 M). Substrates were cleaned sequentially with 2% Hellmanex, ethanol, and deionized water (water repeated three times). The substrates were cleaned in a plasma etcher for 10 min with oxygen as the source gas. A compact TiO^2 (100 nm) layer was deposited via spray pyrolysis; for approximately each 100 cm^2 of substrate, titanium diisopropoxide bis(acetylacetonate) (20 mL of 100 mM, Sigma-Aldrich, 75 wt% in isopropanol) diluted in anyhydrous ethanol was sprayed, with oxygen as the carrier gas, onto the substrate held at 275 °C. A mesoporous layer of TiO_2 paste (1.7 μm thick, Dyesol 18NR-T) was deposited by screen printing, and the substrates were sintered at 500 °C for 30 min following a 3 h ramping. The substrates were treated in a $TiCl_4$ bath (15 mM) incubated at 70 °C for 1 h. After rinsing in deionized water, the substrates were re-sintered at 500 °C as before. The substrates were cooled to and held at 70 °C, after which the devices were immersed in a bath of C106 dye (150 μM, Organica) dissolved in 1:1 *t*-BuOH:ACN by volume. After approximately 18 h, the devices were rinsed in an ACN bath and dried in air. A hole transport matrix solution was made from stock solutions (160 mM spiro-OMeTAD in chlorobenzene, 0.5 M lithium bis(trifluoromethylsulfonyl) imide (Li-TFSI) in ACN, and 2 M *t*-butyl pyridine (tBP) in chlorobenzene) diluted to the desired concentration of each component with chlorobenzene. The hole transport matrix was deposited by spincoating 25 μL of solution per 2 cm^2 of substrate at 1000 RPM for 60 s following a 10 s soak time. After drying in air, in dark, overnight, 200 nm thick silver electrodes were deposited on devices by thermal evaporation at a pressure of £ 10^{-6} Torr with a shadow mask.

Samples for spectroscopic measurements were prepared in the same way in parallel to samples for device measurements. However, the concentration of tBP and Li-TFSI was varied to verify its dependence on observed trends. In addition, FTO was replaced by a quartz substrate and deposition of silver electrodes onto the sample was omitted. Spectroscopy samples were stored in a glovebox, in dark, until one hour prior to measurement.

Solar Cell Characterization: Stimulated AM1.5G sunlight at 100 mW cm^{-2} irradiance was generated using an AAB ABET technologies Sun2000 solar simulator calibrated using an calibrated silicon reference cell with a KG5 filter to minimize spectral mismatch. The mismatch factor was calculated to be less than 1%. JV curves were measured with a Keithley 2400. The solar cells were masked with a metal aperture of ≈0.108 cm^2 to define the active area and to minimize any edge effects, and measured in a light-tight sample holder.

Field Emission Scanning Electron Microscopy (FESEM): FESEM images were obtained with a Hitachi S40300 operating at an accelerating voltage of 5 kV.

Microsecond Transient Absorption Spectroscopy: Microsecond transient absorption spectroscopy was carried out using excitation pulses (550 nm, 7 ns pulse duration, 10 Hz repetition rate) produced by a Nd:YAG laser (EKSPLA, NT340) with a laser fluence on the sample maintained at 50 uJ cm^{-2} per pulse. The probe light used in these experiments (520 nm) was produced by passing the output from a continuous wave xenon arc lamp (150 W) through a monochromator (Acton Research Corporation,

 © 2013 The Authors. Published by WILEY-VCH Verlag GmbH & Co. KGaA, Weinheim

SpectraPro 2150i). The light transmitted through the sample was passed through a second monochromator (Acton Research Corporation, SpectraPro-2300i) before being detected by a fast photomultiplier tube module biased with 750 V (Hamamatsu, R9110). Data traces were recorded on an oscilloscope (Tektronix, DPO3054).

Photoluminescence Upconversion (PLUC) Spectroscopy: The PLUC set-up has been described in detail elsewhere.[47,48] Solid film samples were excited at a photon energy of 3.10 eV and fluence of 30 nJ cm^{-2} with frequency-doubled pulses of 100 fs duration originating from a mode-locked Ti:Sapphire oscillator with 80 MHz repetition rate. The emitted photoluminescence was collected by a pair of off-axis parabolic mirrors and focused onto a β-barium-borate (BBO) crystal mounted on a rotation stage to allow tuning of the phase-matching angle. An intense vertically polarized gate beam (photon energy 1.55 eV) arriving at the BBO crystal at adjustable time delays was used to up-convert the PL at given times after excitation. The resulting sum-frequency photons were collected, dispersed in a monochromator (Jobin Ivon Triax 190), and detected by a liquid-nitrogen cooled CCD. The overall time resolution of the PLUC setup was 300 fs.

Supporting Information

Supporting Information is available from the Wiley Online Library or from the author.

Acknowledgements

The authors thank the Engineering and Physical Sciences Research Council for funding this study. D.J.H. is funded through the Clarendon Award.

Received: April 19, 2013
Revised: June 5, 2013
Published online: September 3, 2013

[1] B. O'Regan, M. Grätzel, *Nature* **1991**, *353*, 737.
[2] B. E. Hardin, H. J. Snaith, M. D. McGehee, *Nat. Photonics* **2012**, *6*, 162.
[3] A. Hagfeldt, G. Boschloo, L. C. Sun, L. Kloo, H. Pettersson, *Chem. Rev.* **2010**, *110*, 6595.
[4] G. Boschloo, A. Hagfeldt, *Accounts Chem. Res.* **2009**, *42*, 1819.
[5] A. F. Nogueira, C. Longo, *Coord. Chem. Rev.* **2004**, *248*, 1455.
[6] A. Yella, H. W. Lee, H. N. Tsao, C. Y. Yi, A. K. Chandiran, M. K. Nazeeruddin, E. W. G. Diau, C. Y. Yeh, S. M. Zakeeruddin, M. Grätzel, *Science* **2011**, *334*, 629.
[7] U. Bach, D. Lupo, P. Comte, J.-E. Moser, F. Weissörtel, J. Salbeck, H. Spreitzer, M. Grätzel, *Nature* **1998**, *395*, 583.
[8] J. Burschka, A. Dualeh, F. Kessler, E. Baranoff, N. Cevey-Ha, C. Y. Yi, M. K. Nazeeruddin, M. Grätzel, *J. Am. Chem. Soc.* **2011**, *133*, 18042.
[9] L. Schmidt-Mende, S. M. Zakeeruddin, M. Grätzel, *Appl. Phys. Lett.* **2005**, *86*, 013504.
[10] D. Poplavskyy, J. Nelson, *J. Appl. Phys.* **2003**, *93*, 341.
[11] J. E. Kroeze, N. Hirata, L. Schmidt-Mende, C. Orizu, S. D. Ogier, K. Carr, M. Grätzel, J. R. Durrant, *Adv. Funct. Mater.* **2006**, *16*, 1832.
[12] L. Schmidt-Mende, M. Grätzel, *Thin Solid Films* **2006**, *500*, 296.
[13] H. J. Snaith, L. Schmidt-Mende, *Adv. Mater.* **2007**, *19*, 3187.
[14] H. J. Snaith, R. Humphry-Baker, P. Chen, I. Cesar, S. M. Zakeeruddin, M. Grätzel, *Nanotechnology* **2008**, *19*, 424003.
[15] I. K. Ding, N. Tetreault, J. Brillet, B. E. Hardin, E. H. Smith, S. J. Rosenthal, F. Sauvage, M. Grätzel, M. D. McGehee, *Adv. Funct. Mater.* **2009**, *19*, 2431.
[16] U. Bach, Y. Tachibana, J.-E. Moser, S. A. Haque, J. R. Durrant, M. Grätzel, D. R. Klug, *J. Am. Chem. Soc.* **1999**, *121*, 7445.
[17] Q. Wang, S. M. Zakeeruddin, M. K. Nazeeruddin, R. Humphry-Baker, M. Grätzel, *J. Am. Chem. Soc.* **2006**, *128*, 4446.
[18] P. Docampo, A. Hey, S. Guldin, R. Gunning, U. Steiner, H. J. Snaith, *Adv. Funct. Mater.* **2012**, *22*, 5010.
[19] Y. M. Cao, Y. Bai, Q. J. Yu, Y. M. Cheng, S. Liu, D. Shi, F. F. Gao, P. Wang, *J. Phys. Chem. C* **2009**, *113*, 6290.
[20] C. J. Barbe, F. Arendse, P. Comte, M. Jirousek, F. Lenzmann, V. Shklover, M. Grätzel, *J. Am. Ceram. Soc.* **1997**, *80*, 3157.
[21] P. Tiwana, P. Parkinson, M. B. Johnston, H. J. Snaith, L. M. Herz, *J. Phys. Chem. C* **2010**, *114*, 1365.
[22] P. Tiwana, P. Docampo, M. B. Johnston, H. J. Snaith, L. M. Herz, *ACS Nano* **2011**, *5*, 5158.
[23] A. Hagfeldt, M. Grätzel, *Chem. Rev.* **1995**, *95*, 49.
[24] B. O'Regan, J. Moser, M. Anderson, M. Grätzel, *J. Phys. Chem.* **1990**, *94*, 8720.
[25] S. A. Haque, Y. Tachibana, D. R. Klug, J. R. Durrant, *J. Phys. Chem. B* **1998**, *102*, 1745.
[26] J. Krüger, R. Plass, L. Cevey, M. Piccirelli, M. Grätzel, U. Bach, *Appl. Phys. Lett.* **2001**, *79*, 2085.
[27] J. Melas-Kyriazi, I. K. Ding, A. Marchioro, A. Punzi, B. E. Hardin, G. F. Burkhard, N. Tetreault, M. Grätzel, J.-E. Moser, M. D. McGehee, *Adv. Energy Mater.* **2011**, *1*, 407.
[28] S. Fantacci, F. De Angelis, M. K. Nazeeruddin, M. Grätzel, *J. Phys. Chem. C* **2011**, *115*, 23126.
[29] B. E. Hardin, A. Sellinger, T. Moehl, R. Humphry-Baker, J.-E. Moser, P. Wang, S. M. Zakeeruddin, M. Grätzel, M. D. McGehee, *J. Am. Chem. Soc.* **2011**, *133*, 10662.
[30] S. A. Haque, T. Park, A. B. Holmes, J. R. Durrant, *ChemPhysChem* **2003**, *4*, 89.
[31] P. Wang, S. M. Zakeeruddin, J.-E. Moser, M. K. Nazeeruddin, T. Sekiguchi, M. Grätzel, *Nat. Mater.* **2003**, *2*, 402.
[32] S. A. Haque, Y. Tachibana, R. L. Willis, J.-E. Moser, M. Grätzel, D. R. Klug, J. R. Durrant, *J. Phys. Chem. B* **2000**, *104*, 538.
[33] N. Hirata, J. E. Kroeze, T. Park, D. Jones, S. A. Haque, A. B. Holmes, J. R. Durrant, *Chem. Commun.* **2006**, *2006*, 535.
[34] M. K. Nazeeruddin, A. Kay, I. Rodicio, R. Humphrybaker, E. Muller, P. Liska, N. Vlachopoulos, M. Grätzel, *J. Am. Chem. Soc.* **1993**, *115*, 6382.
[35] G. Redmond, D. Fitzmaurice, M. Grätzel, *J. Phys. Chem.* **1993**, *97*, 6951.
[36] S. A. Haque, T. Park, C. Xu, S. Koops, N. Schulte, R. J. Potter, A. B. Holmes, J. R. Durrant, *Adv. Funct. Mater.* **2004**, *14*, 435.
[37] S. A. Haque, E. Palomares, B. M. Cho, A. N. M. Green, N. Hirata, D. R. Klug, J. R. Durrant, *J. Am. Chem. Soc.* **2005**, *127*, 3456.
[38] S. N. Mori, W. Kubo, T. Kanzaki, N. Masaki, Y. Wada, S. Yanagida, *J. Phys. Chem. C* **2007**, *111*, 3522.
[39] J. Salbeck, N. Yu, J. Bauer, F. Weissörtel, H. Bestgen, *Synth. Met.* **1997**, *91*, 209.
[40] P. Strohriegl, J. V. Grazulevicius, *Adv. Mater.* **2002**, *14*, 1439.
[41] A. Abrusci, I. K. Ding, M. A. hashimi, T. S. peretz, M. D. McGehee, M. Heeney, G. L. Frey, H. J. Snaith, *Energy Environ. Sci.* **2011**, *4*, 3051.
[42] M. Theander, A. Yartsev, D. Zigmantas, V. Sundström, W. Mammo, M. R. Andersson, O. Inganäs, *Phys. Rev. B* **2000**, *61*, 12957.
[43] J. E. Kroeze, T. J. Savenije, M. J. W. Vermeulen, J. M. Warman, *J. Phys. Chem. B* **2003**, *107*, 7696.
[44] S. R. Scully, M. D. McGehee, *J. Appl. Phys.* **2006**, *100*, 034907.
[45] D. Stauffer, A. Aharony, in *Introduction to Percolation Theory*, CRC Press, Boca Raton, FL, USA **1994**.

© 2013 The Authors. Published by WILEY-VCH Verlag GmbH & Co. KGaA, Weinheim

[46] M. F. Sykes, J. W. Essam, *J. Math. Phys.* **1964**, *5*, 1117.
[47] P. Parkinson, C. Müller, N. Stingelin, M. B. Johnston, L. M. Herz, *J. Phys. Chem. Lett.* **2010**, *1*, 2788.
[48] M. H. Chang, F. J. M. Hoeben, P. Jonkheijm, A. P. H. J. Schenning, E. W. Meijer, C. Silva, L. M. Herz, *Chem. Phys. Lett.* **2006**, *418*, 196.
[49] C. A. Kelly, F. Farzad, D. W. Thompson, J. M. Stipkala, G. J. Meyer, *Langmuir* **1999**, *15*, 7047.
[50] H. J. Snaith, M. Grätzel, *Appl. Phys. Lett.* **2006**, *89*, 262114.
[51] V. I. Arkhipov, P. Heremans, E. V. Emelianova, H. Bässler, *Phys. Rev. B* **2005**, *71*, 045214.
[52] B. A. Gregg, S. G. Chen, R. A. Cormier, *Chem. Mat.* **2004**, *16*, 4586.

© 2013 The Authors. Published by WILEY-VCH Verlag GmbH & Co. KGaA, Weinheim